Channeling of Products in the Hot Atom Reaction H + $(CN)_2$ → HCN/HNC + CN and in the Reaction of CN with CH_3SH

Brian K. Decker† **and R. Glen Macdonald***

Argonne National Laboratory, Chemistry Division, 9700 South Cass Avenue, Argonne, Illinois 60439

Received: March 1, 2001; In Final Form: May 15, 2001

Infrared transient absorption spectroscopy was used to determine the total product branching fractions for the gas-phase hot atom reaction H + $(CN)_2$ → HCN/HNC + CN (a) and the reaction CN + CH_3SH → HCN/HNC + CH_3S/CH_2SH (b) at 293 K. The reactive H atoms had an initial mean translational energy of 92 kJ mol^{-1}, with a 38 kJ mol^{-1} fwhm Gaussian energy distribution. The branching fractions determined for the product channels forming HCN and HNC, respectively, are 0.88 and 0.12 (±0.05) for reaction (a) and 0.81 and 0.19 (±0.08) for reaction (b). The bimolecular rate constant for reaction (b) was measured to be (2.7 ± 0.3) × 10^{-10} cm^3 $molec^{-1}$ s^{-1} at 293 K. The observed product branching fractions for reaction (a) are consistent with the assumption that the average reactive cross sections for the two product channels are approximately equal above their respective energy thresholds. The results for reaction (a) are compared with the related H + XCN (X = Br, Cl) reactions. The large rate coefficient for reaction (b) suggests an interaction via a long-range intermolecular potential, which is facilitated by the small ionization energy of CH_3SH and large electron affinity of CN. The results for reaction (b) are compared with the related reactions of Cl and OH with CH_3-SH.

1. Introduction

Experimental and theoretical work on chemical reaction dynamics traditionally has focused on binary atom−diatom reactions in the gas phase,[1] because these are the simplest and most tractable systems involving the rupture and formation of chemical bonds.[2] The "classical" detailed atom−diatom reaction may be written as A + BC → AB(V', R', T') + C, where the atoms A, B, and C usually are members of the hydrogen/halogen group (H, F, Cl, Br, I), and V', R', and T' represent the disposal of reaction energy respectively into vibrational, rotational, and translational degrees of freedom in the diatomic product.[1] One alternative macroscopic product channel is possible, viz., AC + B, if BC is heteronuclear. Binary reactions involving four atoms can occur between either atom−triatom (A + BCD) or diatom−diatom (AB + CD) pairs, with many more available product channels (including different isomeric forms of the triatomic species) and quantum states (with their corresponding modes of molecular motion) than the three-atom case.[2,3] Due to the development of new experimental techniques in the past 10−15 years, the state-specific preparation and sensitive detection of triatomic and larger molecules has become possible.[2] Likewise, due to advances in theoretical methods based on quantum mechanics, accurate calculations of state-specific dynamics now can be contemplated for reacting systems having more than three atoms.[4] Within the past decade, armed with these new capabilities, workers have begun to extend the study of detailed chemical reaction dynamics to include systems with polyatomic reactants and products.[2]

The cyano radical, CN, is often called a pseudohalogen because of its large electronegativity (between those of F and Cl)[5] and the great strength (∼179 kcal mol^{-1})[6] of its triple bond. The molecular weight of CN also happens to lie between the F and Cl atomic weights. Consequently, in many respects the polyatomic molecule cyanogen, N≡C−C≡N, resembles the homonuclear diatomic halogens, X_2 (X = F, Cl, Br), whose reactions with hydrogen atoms have been well studied.[1] Thus, the hot-atom reaction H + $(CN)_2$ → HCN/HNC + CN is perhaps the simplest five-atom system to compare with the classical **L** + **H**−**H** triatomic systems, where **L** represents a light-mass particle (usually hydrogen), and **H** a heavy-mass particle (e.g., F, Cl, Br, I). The dynamics of this reaction has been investigated in this laboratory, by measuring both the disposal of energy into rotational and translational degrees of freedom in the CN($X\ ^2\Sigma$) ($V' = 0$, R', T') product,[7] and the complete energy disposal for the minor HNC(0 ν_2^1 0), $\nu_2^1 = 0^0, 1^1$, product.[8] Global features of the dynamics, as dictated by **L** + **H**−**H** kinematics, were found to be similar to the analogous triatomic system: H + Cl_2 → HCl + Cl,[7−9] with more than half of the available reaction energy, $\langle E_{avail} \rangle$, appearing as translational motion in the product.[7,8] A major difference was observed in the distribution of $\langle E_{avail} \rangle$ between rotational and vibrational modes of excitation in the minor HNC product, for which $\langle f_R \rangle = 0.32$ and $\langle f_V \rangle = 0.13$,[8] an almost perfect reversal of the situation for H + Cl_2.[8,9] This result can be explained in terms of the potential energy surfaces (PESs) for the related H + NCCl[10,11] and H + NCH[12] systems. Collinear H−NC−X reaction trajectories are highly repulsive on these PESs, and thus HNC is more efficiently formed through bent configurations which impart torque, and hence angular momentum, to the nascent product. In contrast, atom−halogen reactions, H + X_2 (X = F, Cl, Br, I), have collinear or near-collinear transition states,[13] and the released reaction energy imparts little angular momentum. The few data available for the HNCCN PES[14] do not consider the H−NC−CN interaction, but collinear trajectories should be highly repulsive, as they are for the H−NC−X (X = H, Cl) interactions.[8,10−12]

* To whom all correspondence should be addressed. E-mail: macdonald@anlchm.chm.anl.gov.

† Present address: Physical Sciences, Inc., 20 New England Business Center, Andover, MA 01810.

10.1021/jp0108061
Published on Web 06/19/2001

The occurrence of different isomeric product channels represents a fundamental feature of additional complexity in reacting systems with four or more atoms. These product channels represent different distributions of reaction trajectories, and hence, their disposal of reaction energy provides complementary information about the dynamics and the PES of the system. The title reaction is an extremely simple example of this situation, for which only two isomers are possible. In the present work, the branching fractions into the HCN- and HNC-forming product channels of this reaction were determined under bulk conditions at 293 K. A secondary reaction between CN, a product of the title reaction, and CH_3SH, the H-atom precursor, contributed to the observed HCN and HNC. However, the simplicity of the chemical mechanism employed for these experiments permitted these contributions to be differentiated, and the HCN/HNC branching fractions for the CN + CH_3SH reaction were determined as well. The bimolecular rate coefficient for this reaction, which was required in the kinetic analysis to extract the branching fractions, was measured at 293 K. The branching fractions of the title reaction, together with our previous studies on the energy disposal in the CN and HNC products,[7,8] permitted an estimate to be made of the energy disposal in the HCN product, and hence, in the entire system.

2. Experimental Section

Detailed descriptions of the experimental apparatus have been given previously,[15,16] and only a brief description follows. The transverse flow reactor (TFR) consisted of a stainless steel vacuum-tight vessel containing a Teflon box with interior dimensions of 100 × 100 × 5 cm. The TFR was evacuated through a liquid nitrogen trap by a 25 cfm mechanical pump to a base pressure of a few mTorr, with a leak rate of <0.5 mTorr min^{-1}. The pump inlet was throttled to achieve various experimental pressures in the range of 0.75−6.6 Torr. Gaseous reagents were introduced from a separate vacuum system, their partial pressures being determined from their known flow rates and the total pressure in the TFR. The reagents were used directly as supplied by the manufacturers, with the following purities: Ar (AGA Gas, 99.9995%); CH_3SH (Matheson, 99.5%); $(CN)_2$ (Matheson, 98.5%); C_3H_8 (AGA Gas, 99.5%); He (AGA Gas, 99.9995%). The $(CN)_2$ was further purified by pumping on the frozen sample at −78 °C.

A Lambda-Physik Compex 205 excimer laser operating at 248 nm was used to photolyze CH_3SH at the S−H bond,[17] thereby creating translationally hot H-atoms having a mean center-of-mass (COM) kinetic energy of $\langle E_H \rangle = 92$ kJ mol^{-1}, with a Gaussian energy distribution of 38 kJ mol^{-1} full width half-maximum (fwhm).[7] The excimer laser was operated at a nominal power density of 35−50 mJ cm^{-2} $pulse^{-1}$, with a repetition rate of 10 Hz; lower repetition rates of 2−5 Hz were employed at the higher experimental pressures (>2 Torr) to compensate for the slower removal of photolysis and reaction products. Part of the transmitted excimer beam exiting the TFR was monitored with a Molectron J-50 power meter; the transmitted power was used to correct the data for pulse-to-pulse fluctuations in photolysis power, as well as for its gradual decline due to the build-up of UV-absorbing deposits on the optical surfaces.[7] These optics, especially the quartz entrance window and the dichroic UV−IR mirror used to overlap the photolysis and probe laser beams, were removed for cleaning whenever the transmitted power had decreased by ∼25%.

The continuous-wave probe lasers were an Environmental Optical Sensor model 2010-ECU tunable external cavity diode laser, and a Burleigh Model 20 single-mode color center (infrared) laser pumped by a Coherent Innova model 400 Kr^+ laser. The probe laser outputs were aligned and multipassed collinearly through the photolysis region using a White cell adjusted for 8 passes, for a total optical path length of 1136 ± 5 cm. The diode laser was used to monitor the CN radical on individual rovibronic transitions in the (2,0) vibronic bandhead region of the red system ($A^2\Pi \leftarrow X^2\Sigma$) near 790 nm. Similarly, individual rovibrational transitions in the HCN ($X^1\Sigma$) ν_3 (001)←(000) fundamental near 3.0 μm, and the HNC ($X^1\Sigma$) ν_1 (100)←(000) fundamental near 2.7 μm, were monitored with the infrared laser. The absorption transients of CN and one of the triatomic isomers were detected simultaneously after each photolysis pulse. The transmitted intensity of the diode laser probe beam was monitored with a fast Si PIN diode (New Focus). Prior to introduction into the White cell, the infrared probe beam was split into a reference beam and a signal beam, whose intensities were monitored with separate liquid nitrogen-cooled InSb infrared detectors (Cincinnati Electronics). The reference detector output was used in the feedback circuit of an optical modulator (ConOptics) that regulated the intensity of the Kr^+ pump laser; in this manner, the principal source of noise in the infrared probe beam was suppressed. Further suppression of low-frequency noise in both the diode and the infrared probes was achieved by passing the transient absorption signals through a high-pass electronic filter.[15] The frequency responses of the Si PIN diode and the InSb detectors with their associated electronics were better than 20 and 7 MHz, respectively.

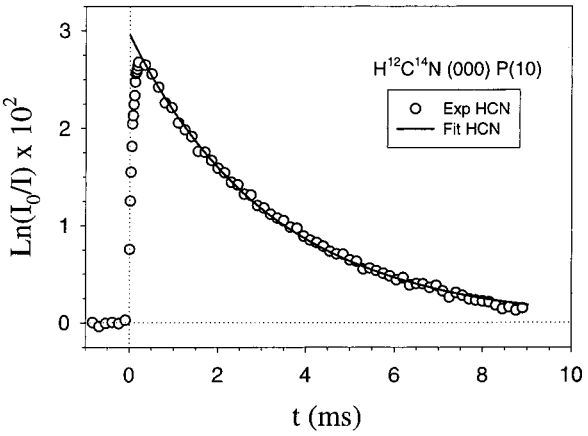

Figure 1. Typical time-resolved absorbance profile for HCN arising from reactions 2a and 3a and monitored with the $H^{12}C^{14}N$ (000) P(10) absorption line. The circles represent experimental data. For clarity, only every third data point for $0 < t < 0.2$ ms, and every 30th data point elsewhere, are shown in the plot. The solid curve is a nonlinear least-squares fit of all data for $t > 0.2$ ms to the simple exponential function, $A\exp(-kt)$, with resulting fit parameters of $A = 296$ and $k = 308$ s^{-1}. The dominant loss process for HCN is diffusion from the photolysis/probe zone. The fit extrapolation to $t = 0$ was used to estimate the nascent concentration of HCN from reactions 2a and 3a (see text). The experimental conditions were $P_{Ar} = 2.45$, $P_{(CN)2} = 0.061$, and $P_{CH3SH} = 0.023$ Torr at 293 K.

Time-resolved and frequency-resolved transient absorption profiles for CN, HCN, and HNC, under varied experimental conditions, were collected at a temperature of 20.0 ± 0.5 °C (293.2 ± 0.5 K). Time-resolved absorbance profiles (see Figures 1 and 2) were obtained by tuning the probe laser to the center frequency of an absorption feature, ν_0, and signal averaging 10^2-10^3 absorption transients with a LeCroy 9410 digital oscilloscope triggered from a fast Si PIN photodiode monitoring the photolysis laser pulses. The baseline probe laser intensity, $I_0(\nu_0)$, was recorded with a Stanford SR-250 boxcar module

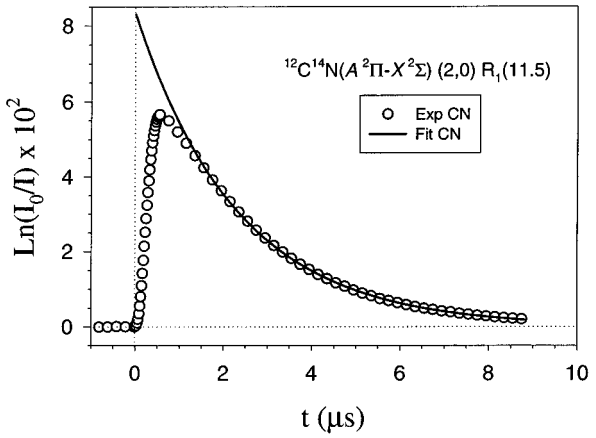

Figure 2. Typical time-resolved absorbance profile for CN arising from reaction 2 and monitored with the $^{12}C^{14}N$ ($A^2\Pi \leftarrow X^2\Sigma$) (2,0) R_1(11.5) absorption line. The circles represent experimental data. For clarity, only every second data point for $0 < t < 0.5$ μs, and every 20th data point elsewhere, are shown in the plot. The solid curve is a nonlinear least-squares fit of all data for $t > 1.4$ μs to the simple exponential function, $A\exp(-kt)$, with resulting fit parameters of $A = 832$ and $k = 4.29 \times 10^5$ s^{-1}. The dominant loss process for CN is reaction 3, with a characteristic time of 2.33 μs. The first-order rate constant, k, from this and other experiments were used to determine the bimolecular rate constant, k_3, for reaction 3 (see text and Figure 5). The experimental conditions were $P_{Ar} = 2.40$, $P_{(CN)2} = 0.084$, and $P_{CH3SH} = 0.024$ Torr at 293 K.

triggered a few hundred microseconds before the photolysis laser. Triggering, collection of data, and other electronic control functions were performed by a laboratory computer. Because the bandwidths of both probe lasers were much narrower than the 293 K Doppler-broadened line profiles of the absorption features, frequency-resolved absorbance profiles providing more accurate absorption measurements than the time-resolved profiles could be obtained[18] (see Figures 3 and 4). Four Stanford SR-250 boxcar modules were used simultaneously to monitor $I_0(\nu)$ and $I(\nu)$ for CN, and $I_0(\nu')$ and $I(\nu')$ for one of the triatomic isomers, where ν and ν' are the frequencies of the diode and infrared probe lasers, respectively. With appropriate time delays determined from the time-resolved profiles, scans were made by stepping the probe laser frequencies through the absorption features in 10−20 MHz increments and accumulating the absorption signal for a fixed number (typically 20−60) of laser shots at each step.

The spectroscopic data needed to calculate line positions for the CN red system[19] and the HCN[20] and HNC[21,22] fundamental transitions were obtained from the available literature. Because HCN and HNC are both moderately light, linear hydrides, their rovibrational transitions are widely separated (several cm^{-1}) relative to their 293 K Doppler widths (~0.008 cm^{-1}),[8] and thus only one absorption feature was recorded per scan. Near-infrared probe laser frequencies were measured to within ±150 MHz accuracy by an evacuated Burleigh WA-20IR wavemeter. Simultaneously with each frequency-resolved infrared absorption scan, the output of a Burleigh CF-500 Etalon, with a free spectral range (FSR) of 150 MHz, was recorded as a function of probe laser frequency. The Etalon FSR was calibrated against the known high-resolution absorption spectrum of acetylene near 3.0 μm,[23] and the Etalon output in turn was used to calibrate the frequency scale for each profile, thereby accounting for variations in the relationship between the scan voltage and the probe laser frequency as the laser was tuned to different absorption features.[8] This frequency-scale calibration allowed the Doppler-broadened line profiles of the absorbing species,

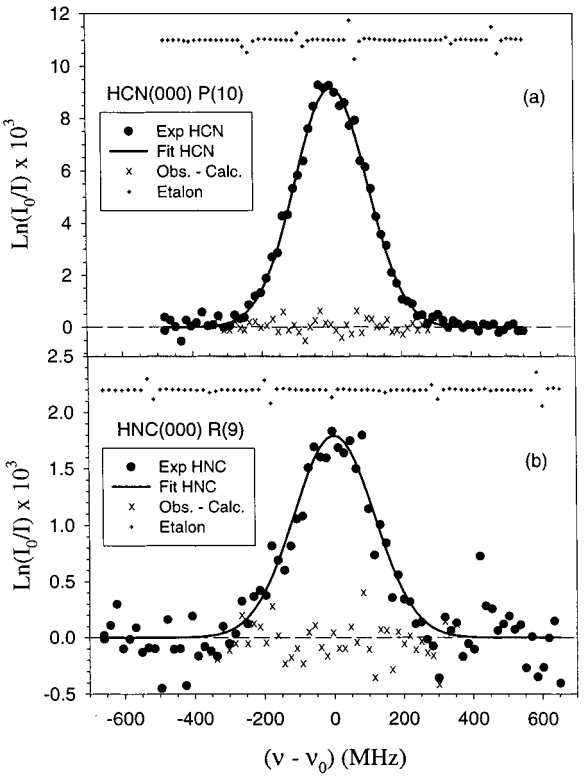

Figure 3. Typical frequency-resolved absorbance profiles for (a) HCN arising from reactions 3a and 4a and monitored with the $H^{12}C^{14}N$ (000) P(10) absorption line, and (b) HNC arising from reactions 3b and 4b and monitored with the $H^{14}N^{12}C$ (000) R(9) absorption line. The filled circles represent experimental data, while the solid curves are nonlinear least-squares fits to the data assuming a Gaussian line shape, with the residues indicated by the "X" symbols. The response of the 150-MHz Etalon over the scan frequency range is shown above the respective data plots in (a) and (b); the Etalon fringes from these traces were used to calibrate the probe laser frequency. The experimental conditions were $P_{Ar} = 0.359$, $P_{C3H8} = 0.958$, $P_{(CN)2} = 0.060$, and $P_{CH3SH} = 0.023$ Torr at 293 K, with a boxcar width of 15 μs centered on delays of (a) 300 μs and (b) 100 μs. At these delay times, the translational energies of the HCN and HNC products were equilibrated to the experimental temperature of 293 K.

and hence their optical densities, to be measured accurately, which was required for the accurate determination of branching fractions.

3. Results

3.1. Reaction Mechanism. Only a few reactions were of importance in the present system, which is described by the following mechanism:

$$CH_3SH \xrightarrow{248\ nm} CH_3S + H^* \quad (1)$$

$$H^* + (CN)_2 \rightarrow HCN + CN \quad f_{2a} \quad (2a)$$

$$\rightarrow HNC + CN \quad f_{2b} \quad (2b)$$

$$CN + CH_3SH \rightarrow HCN + CH_3S/CH_2SH \quad f_{3a} \quad (3a)$$

$$\rightarrow HNC + CH_3S/CH_2SH \quad f_{3b} \quad (3b)$$

$$H^* + M \rightarrow H + M \quad (4)$$

where the f_x (x = 2a,b; 3a,b) are the branching fractions for the indicated product channels. In several experiments, C_3H_8 was added to the gas flow for the purpose of differentiating the

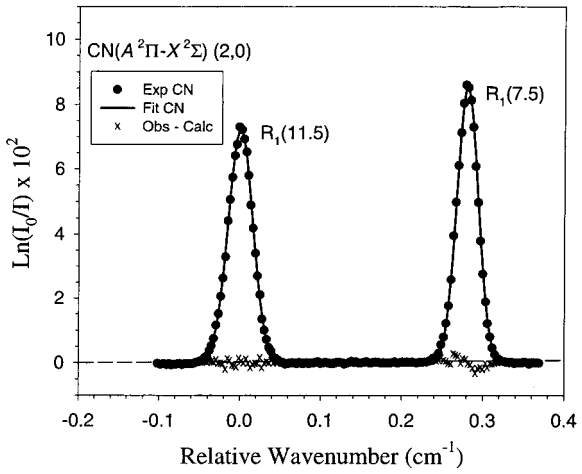

Figure 4. Typical frequency-resolved absorbance profiles for the $R_1(11.5)$ and $R_1(7.5)$ pair of CN(0,J) transitions in the bandhead region of the (2,0) band of the $A^2\Pi \leftarrow X^2\Sigma$ "red" system of CN near 790 nm. The origin of the wavenumber scale is at the center frequency of $R_1(11.5)$. The filled circles represent experimental data, whereas the solid curves are nonlinear least-squares fits to the data assuming a Gaussian line shape, with the residues indicated by the "X" symbols. The experimental conditions were $P_{Ar} = 2.40$, $P_{(CN)2} = 0.084$, and $P_{CH3SH} = 0.024$ Torr at 293 K, with a boxcar width of 0.2 μs centered on a delay of 0.8 μs. From these data, the translational temperatures of the CN $X^2\Sigma$ (0,11.5) and (0,7.5) states, as measured from the fwhm of the Gaussian population line shape, are 409 and 294 K, respectively. Assuming a Boltzmann distribution of rotational states, the ratio of peak absorbances, $A_0(R_1(11.5))/A_0(R_1(7.5))$, indicates a rotational temperature of 380 K.

products of reactions 2 and 3 (see section 3.4). All species were lost by diffusion, which occurred on a time scale of tens of milliseconds at the bath gas pressures employed,[16] whereas reactions (1−4) effectively were complete several microseconds after the photolysis pulse. Relaxation of the HCN and HNC rovibrational states to a Boltzmann distribution at 293 K occurred within 100−300 μs, depending upon the conditions of a particular experiment. Figure 1 illustrates a typical decay profile for HCN, monitored in absorption on the P(10) line of the ν_3 fundamental transition. Diffusion is the dominant loss process for HCN and for HNC.[24] The analogous decay profile for CN, obtained under similar experimental conditions and monitored on the $R_1(11.5)$ line of the (2,0) vibronic band of the red system, is shown in Figure 2.

The photolysis cross-section for CH_3SH at 248 nm is 3.0×10^{-19} cm^2 molec^{-1},[17] implying <1.5% dissociation of CH_3SH under our experimental conditions. Thus, any reaction between CN and CH_3S/CH_2SH can be neglected relative to reaction 3, which is gas-kinetic (see section 3.3). The reaction between CN and $(CN)_2$ is slower by a factor of $\sim 10^5$ than reaction 3 at 293 K.[14] Although other product channels, e.g., the methyl abstraction forming $CH_3CN + HS$, are exothermic for reaction 3, such channels are not observed in the reactions of CH_3SH with Cl[25,26] and with OH,[27] which proceed by rapid H-atom transfer (near the gas-kinetic limit for Cl[25]). These alternative channels are thermodynamically and sterically disfavored relative to simple H-atom transfer.[25] Furthermore, when C_3H_8, which reacts rapidly with CN forming HCN exclusively, was introduced into the reactant mixture in excess of CH_3SH (see section 3.4), no significant change was observed in the total yield of HCN + HNC. Therefore the H-atom transfer product channels, (3a) and (3b), represent the entire product of reaction 3, which is the only significant process removing CN.

The Hess's law reaction enthalpies at 0 K, $\Delta H°_{r0}$, for the active product channels of reactions 2 and 3 are given in Table 1. Both channels of reaction 2 are substantially endothermic with thermal H-atoms at 293 K, and thus only hot atoms with sufficient COM translational kinetic energy, E_H, are reactive. The most probable available reaction energy, $\langle E_{avail} \rangle$, shown in Table 1 for channels 2a and 2b, was calculated from $\langle E_H \rangle = 92$ kJ mol^{-1}, $\Delta H°_{r0}$, and the thermal energy available in the rotation and the low-frequency bending vibrations of $(CN)_2$.[8] Assuming that channel (2b) has no additional potential energy barrier, H-atoms with $E_H \geq 98$ kJ mol^{-1} can contribute to this channel. Yang et al.,[14] using the ab initio BAC-MP4 method, have calculated an activation barrier of ~14 kJ mol^{-1} for channel 2a relative to the products HCN + CN. Thus, H-atoms with $E_H \geq 51$ kJ mol^{-1} can react.

TABLE 1: Summary of the Reaction Energetics for the H + $(CN)_2$ and CN + CH_3SH Systems

reaction system		$\Delta H°_{r0}$	$\langle E_{avail} \rangle$[a]
reactants	products	(kJ mol^{-1})	(kJ mol^{-1})
H[b] + $(CN)_2$[b]	HCN[c] + CN[d]	41 ± 8	+55
	HNC[e] + CN	101 ± 10	−6
CN + CH_3SH[f]	HCN + CH_3S[f]	−157 ± 7	
	HCN + CH_2SH[f]	−129 ± 11	
	HNC + CH_3S	−95 ± 10	
	HNC + CH_2SH	−69 ± 13	

[a] Ref 8. [b] $\Delta H°_{f0}(H) = 216.0$ kJ mol^{-1} (uncertainty much smaller than the precision shown); $\Delta H°_{f0}((CN)_2) = 307.2 \pm 4$ kJ mol^{-1}. Ref. *NIST-JANAF Thermochemical Tables*; Chase Jr., M. W., Ed.; AIP: New York, 1998. [c] $\Delta H°_{f0}(HCN) = 132.3 \pm 4.2$ kJ mol^{-1}. Ref. Berkowitz, J.; Ellison, G. B.; Gutman, D. *J. Phys. Chem.* **1994**, *98*, 2744. [d] $\Delta H°_{f0}(CN) = 432 \pm 5$ kJ mol^{-1}. Ref. Smith, I. W. M. In *The Chemical Dynamics and Kinetics of Small Radicals. Part 1*.; Liu, K. P., Wagner, A., Eds.; World Scientific: Singapore, 1995, p 214. [e] $\Delta H°_{f0}(HNC) = 192.6 \pm 8.2$ kJ mol^{-1}. Ref. Lee, T. J.; Rendell, A. P. *Chem. Phys. Lett.* **1991**, *177*, 491. [f] $\Delta H°_{f0}(CH_3SH) = -3.0 \pm 0.1$ kJ mol^{-1}; $\Delta H°_{f0}(CH_3S) = 31.44 \pm 0.54$ kJ mol^{-1}; $\Delta H°_{f0}(CH_2SH) = 37.7 \pm 2.0$ kJ mol^{-1}. Ref. Ruscic, B.; Berkowitz, J. *J. Chem. Phys.* **1993**, *98*, 2568.

The hot H-atoms created in reaction 1 were relaxed and eventually thermalized by the bath gas (M) in reaction 4. For comparison with future theoretical studies of the dynamics of reaction 2, it is important that the observed product channels arise from H atoms with their initial translational energy distribution. Several observations indicate that this was indeed the case. First, Park et al.[28] have measured the thermalization cross section for H atoms with $E_T = 13$ kJ mol^{-1} colliding with Ar to be $(9 \pm 2) \times 10^{-16}$ cm^2. This is 30 times larger than the estimate of the total reaction cross section, σ_{R2}, for reaction 2 by He et al.[7] Furthermore, σ_{R2} is expected to increase with increasing collision energy as found in similar experimental and theoretical studies on hot H-atom systems.[29−31] Thus, reactive collision events are strongly weighted toward the more energetic H-atoms. Second, within the experimental scatter, there was no difference in the measured branching fractions for a variety of different conditions (see Tables 2 and 3). The concentration of bath gas was always greater than the concentration of $(CN)_2$, >26:1 when only Ar or He was used and >9:1 when C_3H_8 was used. Note that, due to its large manifold of rovibrational states, the thermalization cross section should be much greater for C_3H_8 than for the noble gases.[28] Thus, the collision frequency for reaction 2 relative to that for thermalization was on the order of 10^{-3} to 10^{-2}, and thermalization effectively limited reaction 2 to those H atoms with the initial translational energy distribution. A consequence of the dominance of thermalizing collisions over reactive collisions is that the product concentration should be much smaller than the initial concentration of H-atoms, $[H]_0$, created in the photolysis pulse. Indeed, this was verified experimentally by comparing the measured concentra-

TABLE 2: Summary of the Branching Fraction Measurements for the H + $(CN)_2$ and CN + CH_3SH Reactions (No Propane)

bath gas (M)	P_M (Torr)	P_{C2N2} (Torr)	P_{CH3SH} (Torr)	f_a (HCN)	f_b (HNC)
Ar	5.921	0.071	0.052	0.645	0.355
Ar	2.446	0.061	0.023	0.678	0.322
Ar	2.400	0.084	0.027	0.619	0.381
He	1.770	0.031	0.066	0.663	0.337
Ar	1.587	0.059	0.021	0.766	0.234
Ar	1.559	0.059	0.039	0.636	0.364
Ar	1.459	0.026	0.013	0.732	0.268
Ar	0.727	0.012	0.0064	0.774	0.226
			average:	0.689	0.311
			standard deviation:	0.060	0.060

TABLE 3: Summary of the Branching Fraction Measurements for the H + $(CN)_2$ and CN + CH_3SH Reactions (Propane Added) and the Final Measured Branching Ratios for Reactions 2 and 3

P_{Ar} (Torr)	P_{C3H8} (Torr)	P_{C2N2} (Torr)	P_{CH3SH} (Torr)	f'_a (HCN)	f'_b (HNC)	f_{2a} (HCN)	f_{2b} (HNC)	f_{3a} (HCN)	f_{3b} (HNC)
0	6.380	0.111	0.088	0.802	0.198	0.807	0.193	0.882	0.118
0	2.900	0.052	0.040	0.841	0.159	0.848	0.152	0.841	0.159
1.367	1.003	0.092	0.037	0.892	0.108	0.917	0.083	0.772	0.228
0.984	1.397	0.080	0.024	0.834	0.166	0.842	0.158	0.847	0.153
0	2.272	0.041	0.081	0.821	0.179	0.837	0.163	0.852	0.148
0	1.336	0.022	0.045	0.875	0.125	0.896	0.104	0.793	0.207
0.359	0.958	0.060	0.023	0.889	0.111	0.905	0.095	0.784	0.216
0.721	0.537	0.048	0.019	0.921	0.079	0.949	0.051	0.740	0.260
0	0.989	0.108	0.060	0.886	0.114	0.926	0.074	0.763	0.237
0	1.079	0.020	0.038	0.866	0.134	0.887	0.113	0.802	0.198
			average:	**0.863**	**0.137**	**0.881**	**0.119**	**0.808**	**0.192**
			standard deviation:	0.037	0.037	0.046	0.046	0.046	0.046

tion of the H-atoms that reacted, given by $1/2([HCN]_0 + [HNC]_0]$ (see section 3.4), to an estimate of the initial concentration of H-atoms, $[H]_0$, created in the photolysis pulse. The $[H]_0$ was always at least 2 orders of magnitude larger.

3.2. Determination of the Relative Concentrations of the Transient Species. Determinations of the transition moments, $\langle j|\mu|i\rangle$, for the CN $A^2\Pi \leftarrow X^2\Sigma$ (2,0) vibronic band[32,33] and the HCN $X^1\Sigma$ (001)←(000)[34−36] and HNC $X^1\Sigma$ (100)←(000)[37] fundamental vibrations have been reported in the literature. The values of $\langle j|\mu|i\rangle$ selected from the available data for the present measurements have been tabulated in a previous publication.[18] The integrated line strength, S_{ji}, for these $j \leftarrow i$ transitions can be calculated from the expression[38]

$$S_{ji} = \frac{8\pi^3}{3hc}\,\bar{\nu}_{ji}|\langle j|\mu|i\rangle|^2\,\frac{A_{ji}}{2J+1}F \qquad (5)$$

where h and c have their usual meanings, $\bar{\nu}_{ji}$ is the transition wavenumber, J is the total angular momentum quantum number of the lower (i) state, A_{ji} is the appropriate Hönl−London factor, and F is the appropriate Herman−Wallis factor for the vibrational transitions. For the linear triatomics HCN and HNC, A_{ji} is given by $J + 1$ for an R branch and J for a P branch transition.[39] The F factors were calculated using Herman−Wallis coefficients measured for the HCN ν_3 (1←0) fundamental transition by Smith et al.,[34] and for the HNC ν_1 (1←0) fundamental transition in this laboratory.[22] For CN, whose $A^2\Pi \leftarrow X^2\Sigma$ transition is intermediate between Hund's coupling cases (a) and (b), the A_{ji} were calculated from Earls' formula[40] and normalized by the method of Whiting et al.[41,33]

The absorption cross section at a frequency ν, $\sigma(\nu)$, is related to the integrated line strength by $\sigma(\nu) = g(\nu)S$, where $g(\nu)$ is the normalized-line shape function.[38] At 293 K and the pressures of these experiments (see Tables 2 and 3), $g(\nu)$ has the well-known Gaussian form of a Doppler-broadened absorption profile for the species considered here. The Beer−Lambert absorption law[42] relates the experimentally determined absorbance, $A(\nu)$, to the optical density of the absorbing medium, x_i, through the absorption cross section:

$$A(\nu) = \mathrm{Ln}\left(\frac{I_0(\nu)}{I(\nu)}\right) = x_i\sigma(\nu) \qquad (6)$$

In eq 6, $I_0(\nu)$ is the probe laser intensity and $I(\nu)$ is the transmitted intensity. Because S_{ji} is independent of ν and $g(\nu)$ is normalized, the optical densities of CN, HCN, and HNC in the reaction vessel could be determined by integrating eq 6 and rearranging to obtain

$$x_i = \frac{\int_{-\infty}^{+\infty} A(\nu)\,\mathrm{d}\nu}{S_{ji}} \qquad (7)$$

The integral in eq 7 was evaluated by fitting the experimentally measured frequency-resolved absorbance profiles (see Figures 3 and 4) to a Gaussian line shape function using the commercial software package PEAK FIT. Each fit yielded peak amplitude and fwhm parameters that were used to calculate the area under the absorbance profile.

Because $x_i = l[N_i]$ for a uniformly absorbing medium, where l is the total optical path length and $[N_i]$ the number density of absorbers at ν, the absolute number densities of the absorbing species could be determined in principle. However, because l was identical for all of the absorbing species, the optical densities sufficed for determining relative branching ratios, and thus the additional uncertainty associated with measuring l was avoided. Initial concentrations or optical densities, x_{i0}, were obtained by nonlinear least-squares fitting of the decay portions of the time-resolved absorbance profiles to single-exponential decay functions (see Figures 1 and 2). The fits provided an extrapolation of the peak absorbance to the time origin ($t = 0$) for each species monitored under each set of experimental conditions. The x_i obtained from the frequency-resolved absorbance profiles recorded at various boxcar gate delays were then

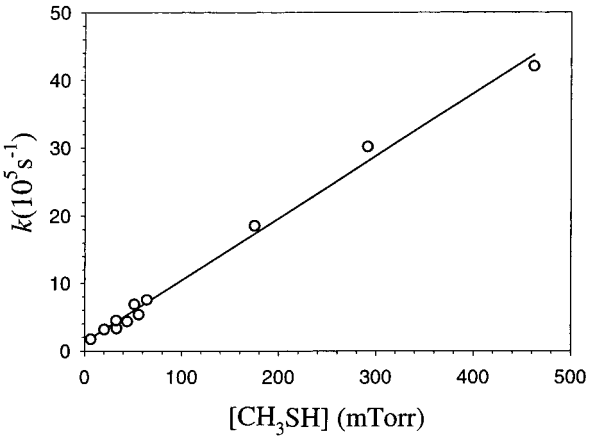

Figure 5. First-order rates, k, for the removal of CN plotted as a function of P_{CH3SH} at 293 K. The linear least-squares fit to the data gives $k_3 = (2.7 \pm 0.2) \times 10^{-10}$ cm^3 molecule^{-1} s^{-1}, whereas the given uncertainty reflects only the precision ($\pm 2\sigma$) in the slope of the least-squares fit line ($r^2 = 0.991$). The total uncertainty in k_3 is estimated to be $\pm$ 0.3 $\times 10^{-10}$ cm^3 molecule^{-1} s^{-1} (see text).

extrapolated using the exponential fits to obtain x_{i0}. For HCN and HNC, which were removed only by diffusion, this correction was small, ~10% or less (see Figure 1). For CN, rotational and translational relaxation occurred on the time scale of reaction 3, and the extrapolation to $t = 0$ involved much greater uncertainty (see Figure 2). Therefore, the branching fractions for reactions 2 and 3 were determined without reference to the initial concentration of CN (see section 3.4).

3.3. Measurement of k_3. The binary rate coefficient for reaction 3, k_3, was determined at 293 K by measuring the first-order decay of CN as a function of [CH_3SH] in the reaction vessel. Because the peak CN concentration was strongly constrained by reactions 1 and 4 (see Section 3.1), reaction 3 was pseudo-first-order in [CN] for all values of [CH_3SH]. The first-order rate constant was obtained at various flows of CH_3SH from a nonlinear least-squares fit of the decay portion of the CN $R_1(11.5)$ temporal absorbance profile (cf. Figure 2) to a two-parameter exponential decay function. The resulting first-order rate constants, k, were plotted against [CH_3SH], as shown in Figure 5. The data were fit by linear regression to the equation $k = k_0 + k_3[CH_3SH]$, where k_0 represents the [CH_3SH]-independent loss processes for CN (predominantly reactions with background impurities). From the least-squares fit, $k_0 = (1.36 \pm 0.52) \times 10^5$ s^{-1} and $k_3 = (9.06 \pm 0.29) \times 10^6$ Torr^{-1} s^{-1}, where the given uncertainties represent the precisions ($\pm 1\sigma$) of the fit parameters. In molecular-cgs units, $k_3 = (2.7 \pm 0.2) \times 10^{-10}$ cm^3 molec^{-1} s^{-1} at 293 K, where the error represents the precision ($\pm 2\sigma$) of the least-squares fit.

A possible source of systematic error in k_3 is the nonthermal energy distribution for CN at early times in the temporal profiles. The nascent translational and rotational temperatures for CN from reaction 2 have been determined to be $T_{trans} = (1389 \pm 109)$ K and $T_{rot} = (885 \pm 45)$ K.[7] Little or no vibrational excitation is expected,[7] and hence under our experimental conditions, thermalization is very rapid. For example, the frequency-resolved absorbance profiles of the neighboring CN $R_1(11.5)$ and $R_1(7.5)$ lines shown in Figure 4 were collected at a boxcar gate delay of 0.8 μs. The translational temperature of the population in the $J = 11.5$ state, as determined from the fwhm of the Doppler-broadened $R_1(11.5)$ absorbance profile, was 409 K, whereas that of the $J = 7.5$ state population was 294 K. The $R_1(11.5)/R_1(7.5)$ peak absorbance ratio suggests a Boltzmann rotational temperature of 380 K. Thus, at 0.8 μs, the CN already was substantially relaxed from its nascent energy distribution. For the determination of k_3, contributions from the nonthermal population of CN were omitted by fitting only the tail portion of the exponential decay in the time-resolved absorbance profile, starting where the absorbance had decreased to ~80% of its peak value (see Figure 2 caption). Very little difference was observed between these fits and those including the entire decay; thus, the decay fits were overwhelmingly weighted toward the thermalized CN.

Other potential sources of systematic error are the determination of CH_3SH concentrations and variations in reactive background impurities (e.g., reagent impurities and photofragments) under different experimental conditions. The flow meters were calibrated by measuring the rate of pressure rise in the known volume of the TFR chamber (see Experimental Section) as a function of the scale flow. Accounting for uncertainties associated with measuring the chamber volume and the pressure change in a given time interval, the accuracy of these flow calibrations is estimated to be within ±3%. The variation in reactive CH_3SH-independent impurity levels from one experimental run to another was responsible for the series of data points having similar slopes (k_3), but different y-intercepts (k_0), in Figure 5. While this affects the apparent scatter of the data, clearly it should not influence the value for k_3 derived from the linear regression. Assuming a systematic uncertainty in the exponential decay constants of ±2% to account for the loss of CH_3SH by photolysis (which is <1.5%; see section 3.1) and any possible CH_3SH-dependent or pressure-dependent background reaction not considered here, the total systematic uncertainty in k_3 is estimated to be ±5% in addition to the precision of the linear regression. Thus, our reported value is $k_3 = (2.7 \pm 0.3) \times 10^{-10}$ cm^3 molec^{-1} s^{-1} at 293 K.

The large value for k_3 indicates that reaction 3 is gas-kinetic. Large rate coefficients frequently have been observed in reactions with CN, particularly with unsaturated hydrocarbons.[43] In some cases, these reactions are faster than the hard-sphere collision rate,[44] especially at lower temperatures (i.e., down to tens of kelvins[45]). Such behavior has been interpreted in terms of "complex formation," in which the particles interact through a long-range intermolecular potential.[44,45] The hard-sphere collision rate coefficient for reaction 3, k_3(hs), can be calculated from estimates of the hard-sphere diameters of CN and CH_3SH.[46] These were obtained from the van der Waals radii of the atoms composing these molecules,[47] together with the bond lengths in CN[48] and CH_3SH,[49] yielding an upper-limit value of $k_3(hs) = 2.5 \times 10^{-10}$ cm^3 molec^{-1} s^{-1} at 293 K. Thus, k_3 is marginally larger than k_3(hs) at room temperature. The analogous reaction of Cl with CH_3SH is also rapid, with an experimentally determined rate coefficient of $(2.0 \pm 0.3) \times 10^{-10}$ cm^3 molec^{-1} s^{-1} at 298 ± 2 K,[25] as compared to its upper-limit hard-sphere value of 1.9×10^{-10} cm^3 molec^{-1} s^{-1}.

3.4. Determination of the Branching Fractions. Because the HCN and HNC relaxed to their Boltzmann rovibrational distributions on a much shorter time scale than diffusion, which was the only significant process removing these species under the present experimental conditions, their yields from reactions 2 and 3 were related to the extrapolated initial concentrations (or optical densities), $[HNC]_0$ and $[HCN]_0$, in a simple way. The sums of the HCN and HNC concentrations created in reactions 2 and 3 are equal because all of the CN radicals created in reaction 2 are assumed to be consumed by reaction 3. For the HNC-forming product channels,

$$f_b = f_{2b} + f_{3b} = \frac{2[HNC]_0}{([HNC]_0 + [HCN]_0)} \quad (8)$$

where f_b is the yield of HNC per $(CN)_2$ molecule from reactions 2 and 3. A similar equation can be written for the yield of HCN. However, the relative contributions from reactions 2 and 3 cannot be determined using the simple mechanism of reactions (1−4) alone. To obtain the desired branching fractions, propane (C_3H_8) was substituted for a portion of the inert bath gas in a number of experiments, such that C_3H_8 was in excess of CH_3SH. Then reaction 9,

$$CN + C_3H_8 \rightarrow HCN + C_3H_7 \quad (9)$$

which has a large binary rate coefficient, k_9, of $(8.3 \pm 0.5) \times 10^{-11}$ cm^3 molec^{-1} s^{-1} at 294 K,[50] became the dominant process removing CN. In a separate study in this laboratory, HNC was searched for, but not detected, as a product of reaction 9 (with CN generated by photolysis of $(CN)_2$ at 193 nm). This nonobservation establishes an upper-limit yield of $\sim 10^{-4}$ for HNC from reaction 9, and thus the only significant product is HCN. Neither HCN nor HNC reacts with propane. The altered yield, f'_b, of HNC is then given by the right-hand side of eq 8. In the limit $R_3/R_9 \rightarrow 0$, where $R_i = k_i[CN][M_i]$ is the rate of reaction i (with $M_3 = CH_3SH$ and $M_9 = C_3H_8$), reaction 3 is "turned off", and the desired branching fractions are simply $f_{2b} = f'_b$ and $f_{3b} = f_b - f'_b$. However, it is difficult to establish the condition that $R_3 \ll R_9$, because $k_3 > k_9$ (see section 3.3 and above) and $[CH_3SH]$ must be kept reasonably large for the production of H-atoms. Thus, the branching fractions are given more generally by

$$f_{2b} = \frac{f'_b}{\bar{R}_9} - \left(\frac{R_3}{R_9}\right) f_b \quad (10)$$

$$f_{3b} = \frac{(f_b - f'_b)}{\bar{R}_9} \quad (11)$$

where

$$\bar{R}_9 = \frac{R_9}{(R_9 + R_3)} = \frac{k_9}{k_9 + k_3 \frac{[M_3]}{[M_9]}} \quad (12)$$

Table 2 lists the yields of HCN (f_a) and HNC (f_b) from the experiments in which propane was not added. Despite the rather large spread in the data, no discernible trend in these yields with bath or reagent gas partial pressure is apparent. Table 3 lists the yields of HCN (f'_a) and HNC (f'_b) obtained from the experiments in which C_3H_8 was added, as well as the branching fractions for reactions 2 and 3 derived using eqs 10−12. From eq 10, f_{2b} was calculated for each value of f'_b using the average value for f_b shown in Table 2. The branching fraction for the HCN-forming product channel, f_{2a}, was calculated simply as $1 - f_{2b}$. The resulting branching fractions for reaction 2 are $f_{2a} = 0.881$ and $f_{2b} = 0.119$ ($\pm$ 0.046), where the uncertainty represents the $\pm 1\sigma$ precision from the 12 experiments shown in Table 3. Here the uncertainty in f_b is negligible, because the term containing f_b in eq 10 makes a small contribution relative to the term containing f'_b. Such is not the case with eq 11, and for the $\pm 1\sigma$ range in f_b, $0.251 \le f_b \le 0.371$, the range of average calculated values (with $\pm 1\sigma$ precision) for f_{3b} from the 12 experiments shown in Table 3 is $(0.126 \pm 0.044) \le f_{3b} \le (0.259 \pm 0.048)$. By adding in quadrature the mean precision of ± 0.046 from these 12 experiments, and the uncertainty of ± 0.067 in the average value for f_{3b}, the branching fractions obtained for reaction 3 are $f_{3a} = 0.808$ and $f_{3b} = 0.192$ (± 0.081).

4. Discussion and Conclusions

Assuming that the channel forming HNC in reaction 2 has no activation barrier and that the HCN-forming channel has a small barrier[14] of 14 kJ mol^{-1} (see section 3.1), the fractions of H-atoms that are initially above the energy thresholds for channels 2a and 2b are 1.00 and 0.30, respectively, as calculated using the thermochemical data in Table 1 and the (92 ± 19) kJ mol^{-1} fwhm Gaussian kinetic energy distribution from reaction 1.[7] With the additional assumption that the average reactive cross sections for channels 2a and 2b are approximately equal above their respective energy thresholds, the predicted branching fractions are $f_{2a}^{(pr)} = 0.85$ and $f_{2b}^{(pr)} = 0.15$, in good agreement with the experimentally determined values of $f_{2a} = 0.88 \pm 0.05$ and $f_{2b} = 0.12 \pm 0.05$. The predicted branching fractions are hardly sensitive to any uncertainty in the threshold for channel 2a. For example, a factor-of-two increase (i.e., to 28 kJ mol^{-1}) in the barrier for this channel leads to predicted branching fractions of $f_{2a}^{(pr)} = 0.84$ and $f_{2b}^{(pr)} = 0.16$. Conversely, neglecting the barrier leaves $f_{2a}^{(pr)}$ and $f_{2b}^{(pr)}$ unchanged.

On the other hand, the possibility of an activation barrier and the uncertainty in the reaction energetics for channel 2b profoundly influence the predicted branching fractions, because the energy threshold for this channel is close to the upper inflection point in the Gaussian energy distribution for the hot H-atoms. As a result, within the ± 10 kJ mol^{-1} uncertainty in ΔH°_{r0} for this channel (see Table 1), the predicted branching fractions range widely, from $f_{2a}^{(pr)}$:$f_{2b}^{(pr)} = 0.68$:0.32 to 0.96:0.04. The assumption that only the *initial* kinetic energy distribution of the H-atoms contributes significantly to the observed product branching overestimates f_{2b}, because channel 2a, with its lower threshold, is more accessible than channel 2b to a partially relaxed distribution of H-atoms. The additional assumption, that the average reactive cross sections for channels 2a and 2b are equal above their respective reaction thresholds, clearly oversimplifies the dynamics of reaction 2, yet leads to predicted branching fractions that are in agreement with those observed. Detailed calculations of the HNCCN PES are not available. However, several stationary points for the CN + HCN reaction have been computed by Yang et al.[14] at the BAC-MP4 level of theory, and indicate that the adduct, NC(H)CN, is bound by ~130 kJ mol^{-1} relative to the H + $(CN)_2$ exit barrier. While it has been noted[8] that this deep potential minimum could facilitate secondary encounters, in which the HNC emerging from reaction 2b reacts with the departing CN to form the more exothermic HCN product, it is also possible that no such effect occurs, and more detailed explorations of the HNCCN reactive PES are needed to resolve this point. If secondary encounters have an appreciable effect, it follows from the assumptions made above that the average reactive cross section for channel 2b via *primary* encounters is greater than for channel 2a.

In previous work from this laboratory, the disposition of reaction energy into the HNC product of channel (2b),[8] and into the CN coproduct of both channels of reaction 2,[7] was determined under near-single-collision conditions. Because channel 2a forming HCN accounts for 88 ± 5% of the product from reaction 2, the measured energy disposal in the CN coproduct largely should reflect the dynamics of this channel. By considering the energy disposal into CN as a linear combination of contributions from channels (2a) and (2b), where

TABLE 4: Estimated Disposition of Reaction Energy in the H + $(CN)_2$ and H + Cl_2 Systems

product channel	$\langle f_T \rangle$	$\langle f_R \rangle$	$\langle f_V \rangle$
CN + HCN/HNC[a]	0.62	0.14	0.24[b]
HCN + CN[c]	0.63	0.12	0.25
HNC + CN[d]	0.55	0.32	0.13
HCl + Cl[e]	0.54	0.09	0.37

[a] Reference 7. [b] Refers to rovibrational excitation in the HCN/HNC coproducts, assuming no vibrational excitation in CN (see ref 7). [c] This work (see Discussion). [d] Reference 8. [e] Reference 51.

TABLE 5: Estimated Cross Sections (in units of 10^{-16} cm^2) to Form the Indicated Products in the Hot-Atom Reactions H + XCN (X = Br, Cl) and H + $(CN)_2$

	reactant		
product	BrCN	ClCN	$(CN)_2$
HCN	0.22	0.5	0.26
HNC	1.5	1.5	0.036
HX	0.026	0.02	

the branching fractions determined in the present work are the coefficients, the energy disposal in the HCN product can be estimated from the data for HNC and CN, as shown in Table 4. As expected, the estimates for HCN are very close to the results for CN. The disposition of reaction energy in the analogous thermal triatomic reaction, H + Cl_2 → HCl(V', R', T') + Cl,[51] is included in Table 4 for comparison. Whereas collinear and near-collinear trajectories contribute most of the reactive flux in the H + Cl_2 reaction,[13] the experimental data accumulated for the H + $(CN)_2$ reaction (refs 7 and 8 and the present work) support the expectation, based on theoretical calculations for the related H + ClCN[10,11] and H + HCN[12] systems, that collinear and near-collinear H−NCCN geometries are highly repulsive, and therefore trajectories that are transverse relative to the NCCN molecular axis contribute most of the reactive flux. The HNC product exhibits a large degree of rotational excitation due to reactive trajectories having bent H−NCCN geometries, which impart torque about the COM of the system.[8] The HCN product is created with much less rotational excitation, because trajectories that approach the C-atoms are closer to the system COM. Note that although the energy disposition in the H + Cl_2 reaction and the HCN-forming channel of the H + $(CN)_2$ reaction are quite similar (see Table 4), they arise from different sets of optimal reaction trajectories relative to the molecular axis. The global features of the energy disposition for the H + $(CN)_2$ reaction are consistent with the **L + H−H** kinematics of the H + Cl_2 and other comparable reaction systems.[8]

In another recent study,[18] we reported the branching fractions for the three accessible product channels of the related hot atom reactions, H + XCN (X = Br, Cl), where the H atoms were generated in the same manner as in the present work. With these cyanogen halides, HNC was the dominant product, with branching fractions of 0.86 ± 0.03 and 0.74 ± 0.03 for X = Br and Cl, respectively. The total cross section for the H + XCN reaction (in units of 10^{-16} cm^2) was estimated to be 1.7, 2.0, and 0.3 for X = Br,[18] Cl,[18] and CN,[7] respectively, within a factor-of-two uncertainty. Table 5 presents the estimated cross sections for the individual product channels in these reactions, obtained from the measured branching fractions and the estimated total reactive cross sections. It is clear by comparison with the H + $(CN)_2$ reaction that the halogen atom of XCN (X = Br, Cl) strongly influences the dynamics. The most complete theoretical study for any of these PESs to date is that of Harding,[10] who calculated 9 transition states and 14 minima on the HClCN surface. These calculations, in agreement with other theoretical and experimental work,[11,52] indicate that the channel forming HCl (+ CN) in the H + ClCN reaction proceeds by direct abstraction via a nearly collinear transition state, with a large activation barrier of ∼91 kJ mol^{-1}.[10] Although no theoretical data are available for the HBrCN PES, the comparable small cross section and energy disposal for the abstraction channel[7] imply a large barrier and near-linear geometry for this reaction as well. The cross section to form HNC is roughly the same for BrCN and ClCN, and much smaller for $(CN)_2$, which reflects, at least in part, the difference in energetics; the HNC channel is accessible to most of the initially hot H-atoms with BrCN and ClCN,[18] but not with $(CN)_2$ (see Table 1). The cross section to form HCN is smaller with BrCN than with ClCN, which has been suggested to indicate geometrical effects due to the larger Br atom.[18] Indeed, it seems likely that the halogen atom is largely responsible for the enhancement of the HNC product relative to the more exothermic HCN product in the XCN (X = Br, Cl) reactions, by deflecting reactive trajectories away from the C-atom.[18]

Although k_3 was measured only at 293 K, the kinetics of the analogous reactions of Cl and of OH with CH_3SH have been determined in the 193−430 K[25] and 244−430 K[53] temperature ranges, respectively. Both exhibit a weak negative dependence on temperature, with $E_a = -1.3 \pm 0.3$ kJ mol^{-1} for Cl[25] and -3 ± 0.8 kJ mol^{-1} for OH.[53] The absence of a significant kinetic isotope effect (with CH_3SD) in either case implies that both proceed principally by an addition−elimination mechanism, in which the radical forms an intermediate adduct with the S-atom.[25,26,54] Wilson and Hirst[26] have located such an adduct on the $CH_3S(Cl)H$ PES, which is bound by 57.1 kJ mol^{-1} relative to the Cl + CH_3SH asymptote, at the MP2 level of theory. Nicovich et al.[25] have demonstrated that the reactivity of Cl with the series of sulfides, RSR′ (R, R′ = H, CH_3), correlates with IE(RSR′) − EA(Cl), where IE represents ionization energy and EA electron affinity. As suggested by these authors,[25] the large electron affinity of Cl (EA(Cl) = 3.61 eV[55]), combined with the relatively small IEs of the sulfides,[55] is likely responsible for long-range electronic interactions that lead to loose, polar transition states and hence to large rate coefficients. The electron affinity of CN is comparable to that of Cl (EA(CN) ≈ 3.8 eV[55]), and thus its kinetic behavior should follow a similar mechanism. An abstraction mechanism also has been predicted to be important in the Cl + CH_3SH reaction,[26] although the lack of an experimentally observed kinetic isotope effect[25] does not support this prediction. With CN, abstraction might be indicated by the product channel forming HNC, because adduct formation via a CN−S interaction is probably much less favorable than the NC−S interaction.

Acknowledgment. The authors thank Dr. G. He and Prof. I. Tokue for their work in the initial stages of these experiments. This work was supported by the U.S. Department of Energy, Office of Basic Energy Sciences, Division of Chemical Sciences, under Contract No. W-31-109-ENG-38.

References and Notes

(1) Polanyi, J. C. *Science* **1987**, *236*, 680.
(2) Schatz, G. C. *J. Phys. Chem.* **1995**, *99*, 516.
(3) Clary, D. C. *J. Phys. Chem.* **1994**, *98*, 10678.
(4) Clary, D. C. *Science* **1998**, *279*, 1879.
(5) Tyler, J. K.; Sheridan, *J. Trans. Faraday Soc.* **1963**, *59*, 2661.
(6) Costes, M.; Naulin, C.; Dorthe, G. *Astron. Astrophys.* **1990**, *232*, 270.
(7) He, G.; Tokue, I.; Macdonald, R. G. *J. Chem. Phys.* **2000**, *112*, 6689.

(8) Macdonald, R. G. *J. Phys. Chem. A* **2000**, *104*, 10202.
(9) Holmes, B. E.; Setser, D. W. In *Physical Chemistry of Fast Reactions. Vol. 2: Reaction Dynamics*; Smith, I. W. M., Ed.; Plenum: New York, 1980; p 83.
(10) Harding, L. B. *J. Phys. Chem*. **1996**, *100*, 10123.
(11) de Juan, J.; Callister, S.; Reisler, H.; Segal, G. A.; Wittig, C. *J. Chem. Phys*. **1988**, *89*, 1977.
(12) ter Horst, M. A.; Schatz, G. C.; Harding, L. B. *J. Chem. Phys*. **1996**, *105*, 558.
(13) Levy, M. R. *Prog. React. Kinet.* **1979**, *10*, 1.
(14) Yang, D. L.; Yu, T.; Lin, M. C.; Melius, C. F. *J. Chem. Phys*. **1992**, *97*, 222.
(15) Bethardy, G. A.; Northrup, F. J.; Macdonald, R. G. *J. Chem. Phys.* **1995**, *102*, 7966.
(16) Bethardy, G. A.; Northrup, F. J.; He, G.; Tokue, I.; Macdonald, R. G. *J. Chem. Phys*. **1998**, *109*, 4224.
(17) Barone, S. B.; Turnipseed, A. A.; Gierczak, T.; Ravishankara, A. R. *J. Phys. Chem*. **1994**, *98*, 11969.
(18) Decker, B. K.; He, G.; Tokue, I.; Macdonald, R. G. *J. Phys. Chem.* A (in press).
(19) Cerny, D.; Bacis, G.; Guelachvilli, G.; Roux, F. *J. Mol. Spectrosc*. **1978**, *73*, 154.
(20) Smith, A. M.; Coy, S. L.; Klemperer, W.; Lehmann, K. K. *J. Mol. Spectrosc*. **1989**, *134*, 134.
(21) Burkholder, J. B.; Sinha, A.; Hammer, P. D.; Howard, C. *J. Mol. Spectrosc*. **1987**, *126*, 72.
(22) Northrup, F. J.; Bethardy, G. A.; Macdonald, R. G. *J. Mol. Spectrosc*. **1997**, *186*, 349.
(23) Auwera, J. V.; Hurtmans, D.; Carleer, M.; Herman, M. *J. Mol. Spectrosc*. **1993**, *157*, 337.
(24) Diffusion actually occurs on a longer time scale than implied by Figure 1, i.e., tens of milliseconds (see ref 16). The decay profile shown in Figure 1 is distorted by use of the digital oscilloscope in its AC signal-input mode, and by high-pass filtering. However, since the branching fractions are determined from *ratios* of the extrapolated initial concentrations, $[HCN]_0$ and $[HNC]_0$, this distortion has a negligible effect under similar filtering conditions for the HCN and HNC decay profiles.
(25) Nicovich, J. M.; Wang, S.; Wine, P. H. *Int. J. Chem. Kinet*. **1995**, *27*, 359.
(26) Wilson, C.; Hirst, D. M. *J. Chem. Soc., Faraday Trans*. **1997**, *93*, 2831.
(27) Butkovskaya, N. I.; Setser, D. W. *J. Phys. Chem. A* **1999**, *103*, 6921.
(28) Park, J.; Shafer, N.; Bersohn, R. *J. Chem. Phys.* **1989**, *91*, 7861.
(29) Kessler, K.; Kleinermanns, K. J. *J. Chem. Phys.* **1992**, *97*, 374.
(30) Bradely, K. S.; Schatz, G. C. *J. Phys. Chem*. **1996**, *100*, 12154.
(31) Bradely, K. S.; Schatz, G. C. *J. Chem. Phys.* **1997**, *106*, 8464.
(32) Knowles, P. J.; Werner, H.-J.; Hay, P. J.; Cartwright, D. C. *J. Chem. Phys.* **1988**, *89*, 7334.
(33) He, G.; Tokue, I.; Macdonald, R. G. *J. Chem. Phys.* **1998**, *109*, 6312.
(34) Smith, M. A. H.; Harvey, G. A.; Pellett, G. L.; Goldman, A.; Richardson, D. J. *J. Mol. Spectrosc*. **1984**, *105*, 105.
(35) Varghese, P. L.; Hanson, R. K. *J. Quant. Spectrosc. Radiat. Transfer* **1984**, *31*, 545.
(36) Smith, I. W. M. *J. Chem. Soc., Faraday Trans.* **1981**, *277*, 2357.
(37) He, G.; Macdonald, R. G. *Chem. Phys. Lett.* **1999**, *301*, 175.
(38) Smith, M. A. H.; Rinsland, C. P.; Fridovich, B. In *Molecular Spectroscopy: Modern Research*; Rao, K. N., Ed.; Academic: Orlando, 1985; p 112.
(39) Herzberg, G. *Molecular Spectra and Molecular Structure III. Electronic Spectra and Electronic Structure of Polyatomic Molecules*; Krieger: Malabar, Florida, 1991; p 226.
(40) Earls, L. T. *Phys. Rev.* **1935**, *48*, 423.
(41) Whiting, E. E.; Schadee, A.; Tatum, J. B.; Hougen, J. T.; Nicholls, R. W. *J. Mol. Spectrosc*. **1980**, *80*, 249.
(42) Kroto, H. W. *Molecular Rotation Spectra*; Dover: New York, 1992; p 68.
(43) Yang, D. L.; Lin, M. C. In *The Chemical Dynamics and Kinetics of Small Radicals. Part 1*.; Liu, K. P., Wagner, A., Eds.; World Scientific: Singapore, 1995; p 164.
(44) Copeland, L. R.; Mohammed, F.; Zahedi, M.; Volman, D. H.; Jackson, W. M. *J. Chem. Phys*. **1992**, *96*, 5817.
(45) Sims, I. R.; Smith, I. W. M. *Annu. Rev. Phys. Chem*. **1995**, *46*, 109.
(46) Johnston, H. S. *Gas-Phase Reaction Rate Theory*; The Ronald Press Company: New York, 1966; pp. 140−141.
(47) Emsley, J. *The Elements*; Clarendon Press: Oxford, 1990.
(48) Huber, K. P.; Herzberg, G. *Molecular Spectra and Molecular Structure IV. Constants of Diatomic Molecules*; Van Nostrand Reinhold: New York, 1979.
(49) Curtiss, L. A.; Nobes, R. H.; Pople, J. A.; Radom, L. *J. Chem. Phys*. **1992**, *97*, 6766.
(50) Hess, W. P.; Durant, J. L., Jr.; Tully, F. P. *J. Phys. Chem.* **1989**, *93*, 6402.
(51) Anlauf, K. G.; Horne, D. S.; Macdonald, R. G.; Polanyi, J. C.; Woodall, K. B. *J. Chem. Phys.* **1972**, *57*, 1561.
(52) Johnston, G. W.; Bersohn, R. *J. Chem. Phys.* **1989**, *90*, 7096.
(53) Tyndall, G. S.; Ravishankara, A. R. *Int. J. Chem. Kinet*. **1991**, *23*, 483.
(54) Butkovskaya, N. I.; Setser, D. W. *J. Phys. Chem. A* **1999**, *103*, 6921.
(55) Mallard, W. G.; Linstrom, P. J. *NIST Webbook*; *NIST Standard Reference Database Number 69*; National Institute of Standards and Technology: Gaithersburg, MD, 1998 (http://webbook.nist.gov).